Wind Energ. Sci. Discuss., https://doi.org/10.5194/wes-2019-9
Manuscript under review for journal Wind Energ. Sci.
Discussion started: 1 March 2019
© Author(s) 2019. CC BY 4.0 License.

eawe european academy of wind energy
Open Access WIND ENERGY SCIENCE DISCUSSIONS

# First Identification and Quantification of Detached Tip Vortices Behind a WEC Using Fixed Wing UAS

Moritz Mauz[1], Alexander Rautenberg[1], Andreas Platis[1], Marion Cormier[2], and Jens Bange[1]

[1]Centre for Applied Geoscience, Eberhard Karls University Tübingen, 72074 Tübingen, Germany
[2]Institute of Aerodynamics and Gas Dynamics, University of Stuttgart, 70569 Stuttgart, Germany

**Correspondence:** Moritz Mauz (moritz.mauz(at)uni-tuebingen.de)

**Abstract.**

Quantifying blade tip vortices helps to understand the process of vortices detaching from the wind converter blade and their development in the wake until finally dissipating in the far wake, contributing to overall turbulence. This is especially interesting for set-ups of numerical simulations when setting the spatial resolution of the simulation grid.

The MASC MK 3 (Multi-purpose Airborne Sensor Carrier Mark 3) UAS (Unmanned Aircraft System) by the University of Tübingen measured atmospheric and meteorological quantities during the HeliOW campaign in July 2018 data behind a wind energy converter (WEC) (Enercon E-112) north of Wilhelmshaven, Germany, at the Jade Wind Park. Aside turbulence distribution, air temperature, humidity and the three wind components u, v, w in front of the WEC and in the wake were measured. By evaluation of the wind components, detached blade tip vortices were identified in the time series. The presented data were captured under a dominating marine stratification about 2 km from the North Sea coast line with northern wind direction. The measured vortices are compared to the analytical Burnham-Hallock model for two vortices spinning in opposite direction. The model has its origin in aviation, where it describes two aircraft wake vortices. It will be shown that the BH model can be used to describe wake vortices behind a WEC. An evaluation method is presented to measure detached tip vortices with a fixed wing UAS. Also an improvement for the model in WEC wake use will be proposed.

*Copyright statement.* TEXT

## 1 Introduction

Since the politically induced 'Energiewende' (exit from nuclear and fossil energy sources) in the late 1990s in Germany, the wind energy sector has been growing. Not only in the amount of installed wind energy converters (WECs) but also in their single capacity and diversity. A modern off-shore WEC delivers up to 9 MW of power in ideal conditions. The constant enhancements of the concept of harvesting energy from wind lead to a wide field of applications for WECs, e.g. in homogeneous conditions off-shore as well as in complex terrain further inland. In research and development numerical simulation of the wind velocity field of a WEC and its produced turbulence is an important tool that gives valuable insights of pressure and velocity distributions

Wind Energ. Sci. Discuss., https://doi.org/10.5194/wes-2019-9
Manuscript under review for journal Wind Energ. Sci.
Discussion started: 1 March 2019
© Author(s) 2019. CC BY 4.0 License.

eawe european academy of wind energy
Open Access WIND ENERGY SCIENCE DISCUSSIONS

around a turbine blade and nacelle as well as in the wake. A numerical model increases its validity when it is backed by real world in-situ data. Not least, because of improvements that can flow back into the model, once measured data has revealed some possible tweaks and enhancement to the prior model. Numerical simulation might under predict peak vorticity and radii of wake vortices, especially when the grid size of the simulation is not sufficient (Kim et al., 2016). Another mean of studying WEC wakes are wind tunnel experiments that try to recreate wake patterns in a smaller scale (e.g. Bartl et al. (2012) or Vermeer (1992)). While in the early days of wind tunnel experiments the wake has been visualised by smoke trails, PIV (Particle Image Velocimetry) measurements have increased the resolution and accuracy of wind tunnel experiments drastically (e.g. resolving Reynolds shear stress and turbulent kinetic energy, Zhang et al. (2012)).

The MASC Mk 3 system allows in-situ high frequency measurements of the atmospheric flow and its transported properties. A detailed description of the UAS and its instruments can be found in Wildmann et al. (2014a) and Wildmann et al. (2014b). The latest iteration MASC Mk 3 is using an improved IMU (Inertial Measurement Unit) and positioning system. The lateral positioning accuracy is now in a range of 2 $\mathrm{cm}$, whilst the vertical path accuracy has also improved by approximately $0.45\ \mathrm{m}$ through implementing revised design elements in the fuselage allowing a more stable flight path and using a more precise GPS.

For this study of the near wake of a WEC an Enercon E-112 prototype located at the Jade Wind Park north of Wilhelmshaven at the German North Sea coast has been chosen. This specific converter and its location near the coast is comparable with off-shore converters in marine flow which was a requirement when choosing the WEC. The measurements are part of the HeliOW project, in which the atmospheric turbulence in front of and in the wake of a WEC are the foundation of a chain of numerical simulations. The project aims for save helicopter flight paths in off-shore wind energy parks. The numerical simulation chain also includes flight-mechanical simulations (provided by Technical University Munich and DLR Braunschweig) of helicopters interacting with turbulence generated by WECs. The helicopter flight simulations are coupled with a numerical simulation of the marine flow over an off-shore 4.5 MW wind energy converter. The WEC simulations are done by the Univerity Stuttgart.

A WEC, especially in a stable marine ABL (atmospheric boundary layer), acts as a turbulence generator. The added turbulence has two main sources. On the one hand the increased wind shear in the wake that results from the wind deficit in the near wake and the low pressure bulb that develops behind the WEC nacelle. On the other hand turbulence is created by expansion and dissipation of detached blade tip vortices that transfer their kinetic energy to the surrounding flow. A proper understanding of these vortices and their inducing load onto the converter blade is of great importance for future enhancement of life span and working loads of wind energy converters. Blade tip vortices follow a helical pattern into the wake, detaching from each converter blade. These detached eddies can be measured with the mounted five-hole-probe on the MASC UAS. Subramanian et al. (2015) measured the presence of tip vortices via pressure fluctuations qualitatively in a flight pattern along the wake, also using a small UAS. In this study an evaluation method is presented to measure the core radius and maximum tangential velocity of a tip vortex $r_c$ using in-situ wind measurements from flight patterns perpendicular to the mean wind velocity.

Wind Energ. Sci. Discuss., https://doi.org/10.5194/wes-2019-9
Manuscript under review for journal Wind Energ. Sci.
Discussion started: 1 March 2019
© Author(s) 2019. CC BY 4.0 License.

**Figure 1.** Research UAS MASC Mk 3 shortly before lift-off. (Photo taken by the author).

**Table 1.** Characteristics of the MASC Mk 3 UAS at the HeliOW campaign.

| | |
|---|---|
| wingspan | 4 m |
| total weight | $\approx$ 7 kg |
| sci. payload | $\approx$ 1 kg |
| cruising speed | 19 m s$^{-1}$ |
| endurance | up to 2 h |
| propulsion | electrical pusher engine |
| take-off | bungee or winch |

## 2 Measurement system and measurement site

### 2.1 Research aircraft

The research UAS MASC Mk 3 (cf. Fig. 1 and Tab. 1) is a fixed wing airborne measurement system of the University of Tübingen that has been used in several measurement campaigns and has been described by Wildmann et al. (2014a, b). The third iteration of this platform features some changes to the fuselage. The electrical pusher motor has moved from a centre position behind the wings to the tail, accelerating the aircraft along the centre axis increasing flight stability. The time span in which the presented data was captured was about 15 minutes. It can be expected that atmospheric conditions (wind direction and speed) did not change during this period.

Aside the manual changes to the platform the former ROCS autopilot operating on the MASC Mk 2 system has been changed to the Pixhawk 2.1 autopilot. This is an independent open-hardware and open-source autopilot project (www.pixhawk.org). The Pixhawk autopilot is equipped with RTK GPS, which enables a track accuracy in the centimetre range.

Wind Energ. Sci. Discuss., https://doi.org/10.5194/wes-2019-9
Manuscript under review for journal Wind Energ. Sci.
Discussion started: 1 March 2019
© Author(s) 2019. CC BY 4.0 License.

**Figure 2.** Research UAS MASC Mk 3 in front of an Enercon wind energy converter at the Jade Wind Park in July 2018. (Photo taken by the author).

### 2.2 Measurement site

Figure 3 shows the location of the measurement site in the north-west of Germany and the flight tracks of the MASC Mk 3 UAV around the Enercon E-112 converter. Both tracks are part of a rectangular flight pattern around the WEC in anti-clockwise direction. For the wake data evaluation only the data captured along the southern flight tracks (orange path in Fig. 3) are used.

The WEC is the most powerful converter in the Jade-Wind-Park north of Wilhemshaven, Germany. The particular converter is a former near-shore prototype with a diameter of 114 $\mathrm{m}$ delivering up to 4.5 $\mathrm{MW}$ of electrical power and thus comparable to an actual off-shore WEC. The Jade-Wind-Park is located about 2 $\mathrm{km}$ from the North Sea coast line and a maritime influence in the wind profile can be expected.

Apart from surrounding WECs (to the south of the E-112 WEC) power lines to the east and north and industrial buildings to the north and north-east (not in the picture) restricted the flight path to the ones depicted in Fig. 3.

Wind Energ. Sci. Discuss., https://doi.org/10.5194/wes-2019-9
Manuscript under review for journal Wind Energ. Sci.
Discussion started: 1 March 2019
© Author(s) 2019. CC BY 4.0 License.

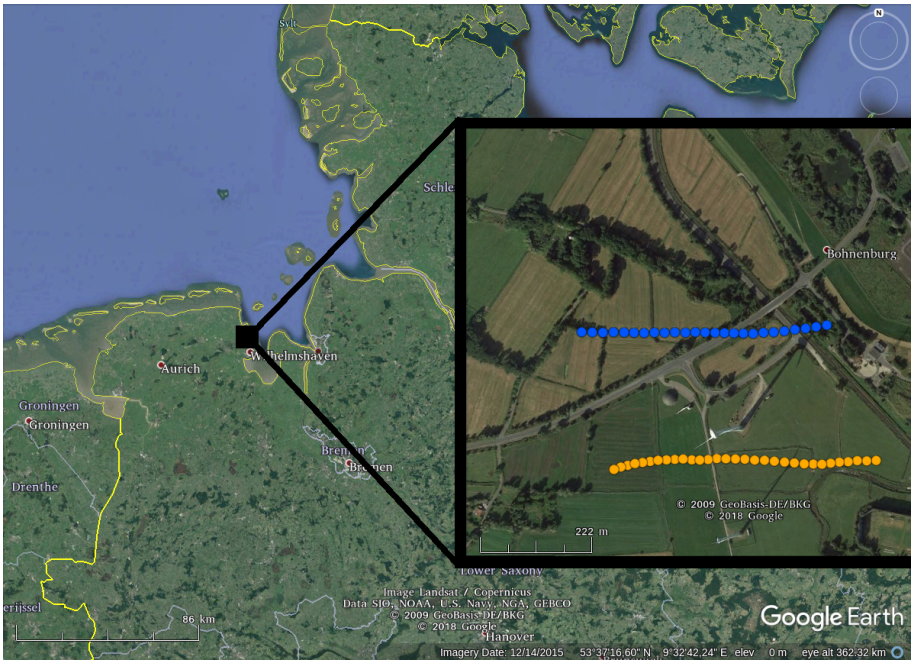


**Figure 3.** Location of the E-112 WEC in the north-west of Germany near the North Sea coast. MASC flight tracks in front (blue) and in the wake (orange) of the E-112 with northern main wind direction (5 degree north that day). On the Google Earth image the WEC is oriented toward south-easterly wind direction.

## 3 Methods

With the goal to measure detached tip vortices behind a WEC, it is helpful to have a first understanding of the behaviour of those vortices. Fig. 4 shows the helical vortex pattern forming behind a WEC, by representing the iso-surfaces of the $\lambda_2$-criterion of detached tip vortices from CFD simulation. The fully resolved URANS simulation has been performed at the University of Stuttgart with the compressible flow solver FLOWer (Kroll and Fassbender, 2005), using the Menter SST (Menter, 1994) turbulence model. The modelled rotor is a stand alone generic recreation of the Enercon E-112 WEC rotor, based on free access airfoil data. For more details regarding the numerical methods, please refer to Cormier et al. (2018) in which the same methods have been applied and described. Figures 5 and 6 give a qualitative impression of the presence of the WEC wake. In both, horizontal wind velocity and turbulence kinetic energy (TKE) the wake and its effects are visible. Farther downstream the helical pattern will start to meander and the symmetrical pattern will dissipate into turbulence. In the near vicinity of the WEC nacelle these vortices follow a helical pattern. The helical structure is shown simplified by a ring vortex in Fig. 7. Note that the tangential velocity in this sketch can be split in its horizontal components at hub height (nacelle height). Here the $y$ axis points north (parallel to main wind direction) similar to the conditions at the HeliOW campaign (cf. Fig. 3) and the $x$ axis points east along the UAS flight path. When measuring at hub height the tip vortex has ideally no $w$ component (Fig. 7). The

Wind Energ. Sci. Discuss., https://doi.org/10.5194/wes-2019-9
Manuscript under review for journal Wind Energ. Sci.
Discussion started: 1 March 2019
© Author(s) 2019. CC BY 4.0 License.

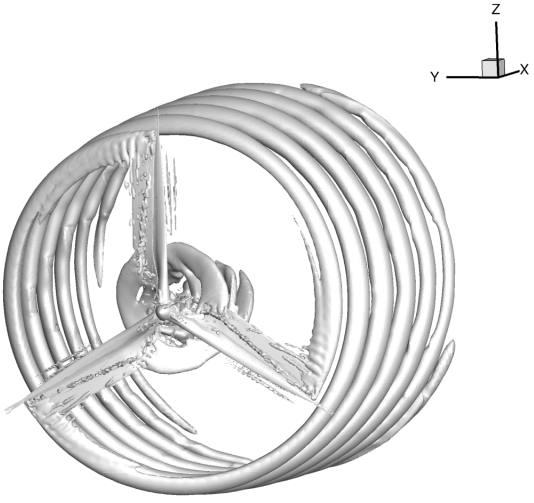


**Figure 4.** Iso-surfaces of detached blade tip and root vortices following the $\lambda_2$ criterion for vortex identification. Here the $x$ axis follows the main wind direction. Numerical simulation of a generic recreation of an E-112 4.5 MW converter.

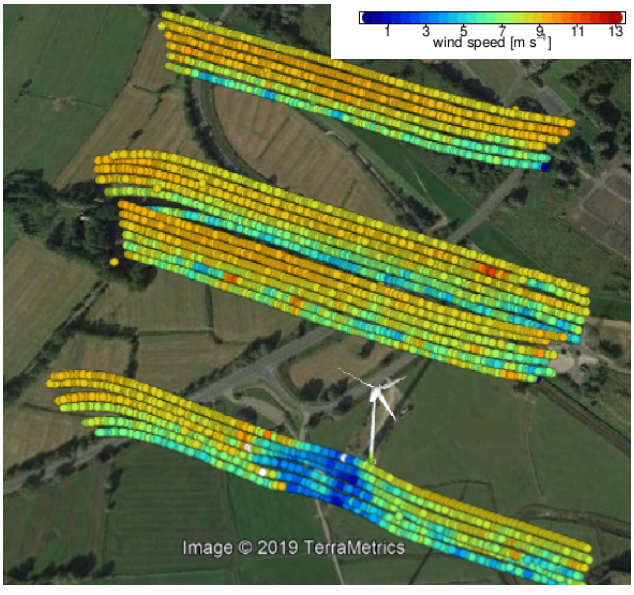


**Figure 5.** Visualisation of the horizontal wind measurements at different flight leg altitudes (from 85 m to 185 m above ground in 20 m steps) and different distances to the WEC (1D, -1D, -2D and -4D). Significant wind deficit 1 D behind the WEC E-112. At this day the wind direction was about 30° north. Image generated in Google Earth.

red rectangle indicates a change of perspective, showing a top view of a vortex spinning in the $x-y$ plane. For later evaluations the coordinate system has been rotated into the main wind direction.

Wind Energ. Sci. Discuss., https://doi.org/10.5194/wes-2019-9
Manuscript under review for journal Wind Energ. Sci.
Discussion started: 1 March 2019
© Author(s) 2019. CC BY 4.0 License.

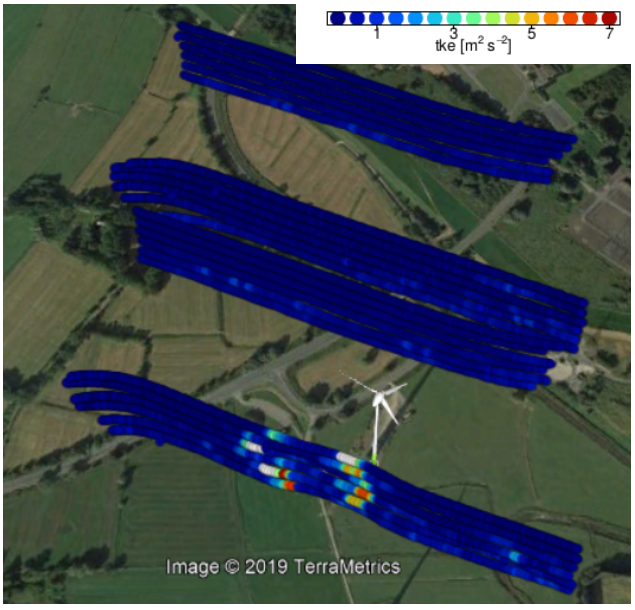


**Figure 6.** Visualisation of the turbulence kinetic energy (TKE) from the same measurements as in Fig. 5. Blue areas represent low turbulence and red the highest measured. At 1D the presence of the wake and the produces turbulence by the tip vortices is visible. Image generated in Google Earth.

### 3.1 Vortex model

Previous efforts to define a vortex were reviewed e.g. by Jeong and Hussain (1995), comparing several definitions with data from direct numerical simulations and exact solutions of the Navier Stokes Equations. A universal definition of a vortex or a generally applicable model does not exist. Assuming incompressible flow and an irrotational velocity field, where the curl of the gradient of the velocity is zero, potential theory is applicable. Considering potential flow, the circulation $\Gamma$, representing the strength of a vortex, around a contour $C$, can be connected to the vorticity flux by Stokes' theorem. For any surface $S$ that spans the curve $C$ and $d\boldsymbol{I}$ being an infinitesimal tangential element along $C$,

$$\Gamma = \oint_C \boldsymbol{V_t} \cdot \mathrm{d}\boldsymbol{I} = \int_S \boldsymbol{\omega} \cdot \boldsymbol{n} \, \mathrm{d}S. \tag{1}$$

The circulation $\Gamma$ is the line integral of the tangential velocity along the curve $C$ which is equal to the vorticity flux $\omega = \nabla \times V_\mathrm{t}$ through the surface $S$, with $\boldsymbol{n}$ being the normal vector of the surface.

A circular integration in a cylindrical polar coordinate system with the azimuthal angle $\phi$ and the radius $r$ yields:

$$\Gamma(r) = \int_0^{2\pi} \int_0^{r} \boldsymbol{\omega}(r, \phi) r \, dr \, d\phi \tag{2}$$

Wind Energ. Sci. Discuss., https://doi.org/10.5194/wes-2019-9
Manuscript under review for journal Wind Energ. Sci.
Discussion started: 1 March 2019
© Author(s) 2019. CC BY 4.0 License.

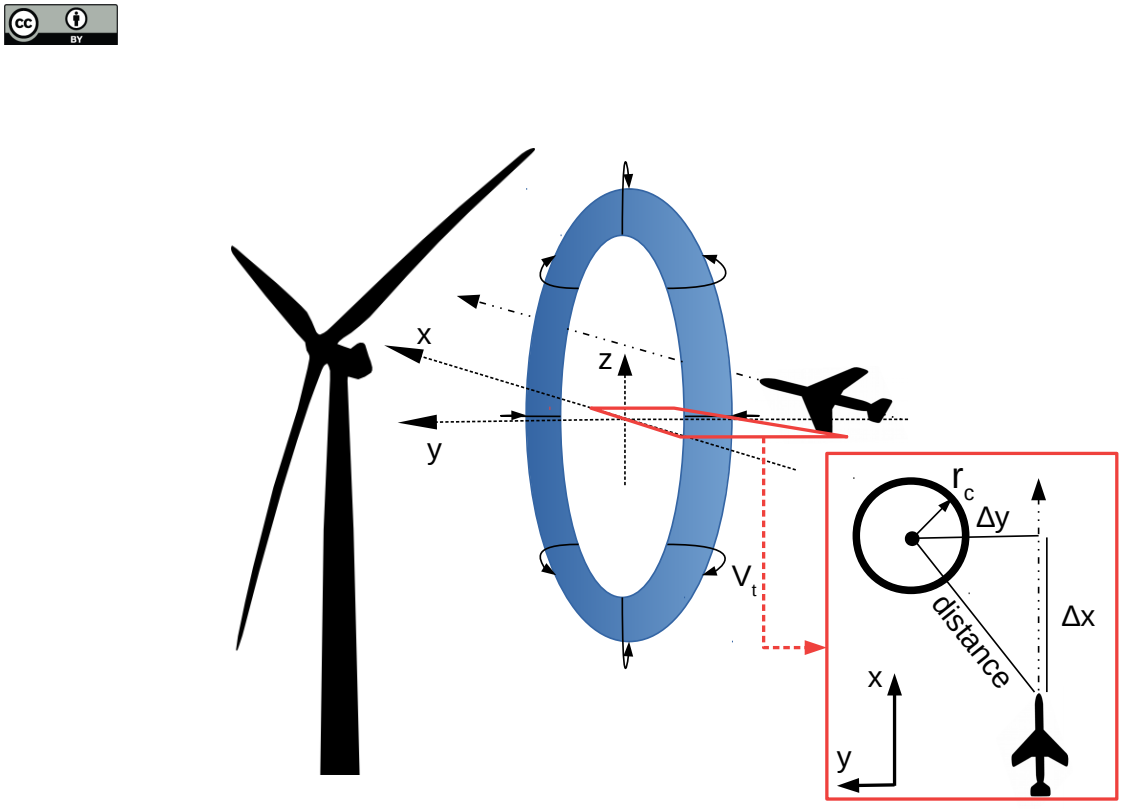


**Figure 7.** Simplified sketch of a vortex pair passed by the UAV to the right. In reality it would rather have a helical pattern than a ring shape. Velocities and axis according to meteorological standards, therefore axis and orientation according to the in-situ conditions. $y$ axis pointing north, $x$ axis pointing east. At hub height the $w$ component (along $z$ axis) vanishes. The red rectangle illustrates a top view of a tip vortex with distance $\Delta y$ to the UAS.

For a two dimensional, axisymmetric vortex, the circulation

$$\Gamma(r) = 2\pi r V_{\mathrm{t}}(r) \tag{3}$$

is a simple function of the radius and the tangential velocity $V_{\mathrm{t}}$. Since real vortices in fluids experience viscous effects, the structure of detaching tip vortices of the blade of WEC cannot be sufficiently described by Equation 3. Close to the centre of the vortex, lower tangential velocities persist, increasing to their maximum at the core radius $r_c$ of the vortex and decreasing again for further distances $r$. To account for that, in the context of WEC and also for detaching tip vortices from the wings of aircraft, several analytical models were suitable.

Since in this study detached vortices of a WEC converter are treated similar to aircraft wake vortices, a few similar model approaches were possible. A comparison of analytical vortex models for tip vortices created by aircraft has been done by Ahmad et al. (2014). Also Fischenberg (2011) measured wake vortices created by the VFW 614 ATTAS manned aircraft (DLR Braunschweig) and compared the results to two similar vortex models proposed by Lamb (1939) and Burnham and Hallock (1982). Fischenberg concludes that both models show the ageing processes of a vortex wake known from theory. In general the model by Burnham-Hallock shows a slightly better agreement in circulation and tangential velocity to the conducted

Wind Energ. Sci. Discuss., https://doi.org/10.5194/wes-2019-9
Manuscript under review for journal Wind Energ. Sci.
Discussion started: 1 March 2019
© Author(s) 2019. CC BY 4.0 License.

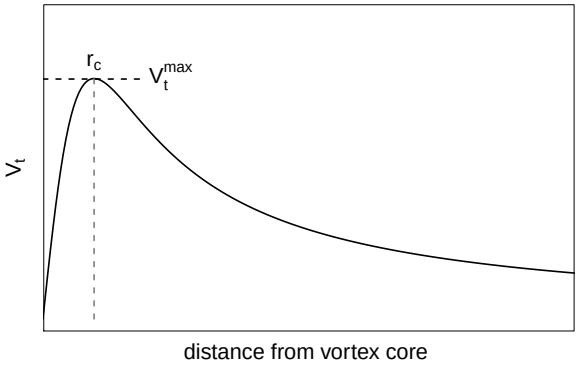


**Figure 8.** Qualitative plot of the tangential velocity from the vortex core outwards. The tangential velocity increases from zero (left) to a maximum at a distance $r_c$ and decreases to zero for large distances (to the right).

measurements by Fischenberg. Also Vermeer (1992) uses the Burnham-Hallock vortex model successfully to describe WEC wake vortices. According to these findings and its simplicity it has been decided to use the analytical solution for wake vortices by Burnham-Hallock in this study.

The Burnham-Hallock model provides a solution for two vortices spinning in opposite direction, as found in an aircraft wake. A similar constellation of vortex pairs can be found in a WEC wake at hub-height (cf. Fig. 7) along the $x$ axis.

Following the Burnham-Hallock model a vortex is described by its circulation $\Gamma$, tangential velocity $V_t$ and its core radius $r_c$. The tangential velocity is the velocity of the air circling the vortex centre and is a function of the distance $r$ to the vortex core.

$$V_t(r) = \frac{\Gamma}{2\pi} \frac{r}{r_c^2 + r^2}. \tag{4}$$

The core radius $r_c$ is defined as the distance from the vortex centre (or core) at which the tangential velocity is at its maximum (circular symmetry). So the radius $r_c$ is also the radius at which the surface integral (cf. Eq. 1) is maximal, considering a circular surface. For $r = r_c$ the maximum tangential velocity becomes (Eq. 5)

$$V_{t,\,max} = \frac{\Gamma}{4\pi r_c}. \tag{5}$$

Figure 8 shows the tangential velocity $V_t$ distribution of a Burnham-Hallock modelled vortex with the highest tangential velocity at the distance $r = r_c$. The distribution is circle symmetric with the vortex core ($r = 0$) in its centre.

In order to estimate the circulation and size of $r_c$ from transects through the vortices with MASC in the wake of a WEC, the following procedure is proposed.

Wind Energ. Sci. Discuss., https://doi.org/10.5194/wes-2019-9
Manuscript under review for journal Wind Energ. Sci.
Discussion started: 1 March 2019
© Author(s) 2019. CC BY 4.0 License.

eawe european academy of wind energy
Open Access WIND ENERGY SCIENCE DISCUSSIONS

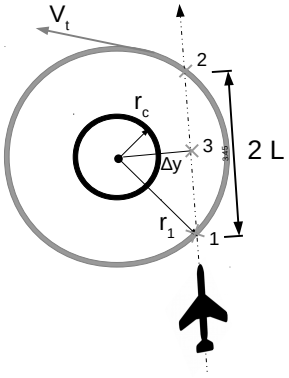


(a) (b)

**Figure 9.** Schematic of the UAS passing a vortex in the horizontal plane (top down view). Two different cases have to be distinguished. The closest distance to the vortex $\Delta y > r_c$ (a) and the passing distance being $\Delta y < r_c$ (b).

### 3.2 Evaluation method

As shown above it is likely to measure tip vortices in hub height that reduce to a two dimensional problem, simply due to their physical presence and orientation at hub height. The vortices can therefore be considered of circular shape rotating in the horizontal plane thus the vertical component $w$ vanishes. So after subtracting the mean wind $v_\infty$ the vortex tangential velocity is

$$\boldsymbol{v} - \boldsymbol{v_\infty} = \boldsymbol{v'} = (u', v', 0). \tag{6}$$

The norm of the tangential velocity then is

$$V_\mathrm{t} = \sqrt{u'^2 + v'^2}. \tag{7}$$

When measuring with a UAS the measurement can be considered a snap shot of the in-situ conditions. Figure 9 differentiates between two different scenarios of the UAS passing a vortex. Both shown from a top view. In Fig. 9a the UAS passes the vortex at its closest distance ($\Delta y$), marked point 3 in the sketch, with $\Delta y > r_c$ thus the vortex core radius is not reached. Point 1 and 2 mark the position of two corresponding tangential velocities of identical absolute value when approaching the vortex and moving away from it again. The measured signal is similar to the dashed black line in Fig. 10 that is an example for $\Delta y = 2r_c$. From such data only point 3 can be identified, since it is the point at which the measured tangential velocity is at its maximum. Point 1 and 2 are somewhere left and right of the maximum with $L$ being unknown. There are indefinite combinations of $\Gamma$ and

Wind Energ. Sci. Discuss., https://doi.org/10.5194/wes-2019-9
Manuscript under review for journal Wind Energ. Sci.
Discussion started: 1 March 2019
© Author(s) 2019. CC BY 4.0 License.

eawe european academy of wind energy
Open Access WIND ENERGY SCIENCE DISCUSSIONS

$r_c$ that could describe the vortex using Eq. 4.

$$V_{t,2} = V_{t,1} = \frac{\Gamma}{2\pi} \frac{r_1}{r_c^2 + r_1^2} \tag{8}$$

$$V_{t,\Delta y} = \frac{\Gamma}{2\pi} \frac{\Delta y}{r_c^2 + \Delta y^2} \tag{9}$$

$$r_1^2 = r_2^2 = L^2 + \Delta y^2 \text{ (Pythagorean theorem)} \tag{10}$$

The three equations 8, 9, 10 are known to describe the velocities and geometry of the measurement. $V_{t,1}$ ( $V_{t,2}$) is the tangential velocity at the point 1 (and 2). Since there are four unknown parameters $\Gamma$, $r_c$, $L$, and $r_{1,2}$ the problem is not solvable.

In case $\Delta y < r_c$ the sketch in Fig. 9b applies. The measured tangential velocity now provides a distinct feature; a double peak in the horizontal wind measurement. This double peak can be lead back to passing the maximum tangential velocity at $r = r_c$ at position 1 and 2. Since the tangential velocity decreases from that point inwards (towards the vortex core), the velocity at point 3 is a local minimum, leading to a visible 'dent' in the data (cf. red line in Fig. 10). Additionally the ground speed of the UAS is known, hence the distance $L$ can be calculated. The three equations previously described above then become:

$$V_{t,2} = V_{t,1} = V_{t,\max} = \frac{\Gamma}{2\pi} \frac{r_c}{r_c^2 + r_c^2} = \frac{\Gamma}{4\pi r_c} \tag{11}$$

$$V_{t,\Delta y} = \frac{\Gamma}{2\pi} \frac{\Delta y}{r_c^2 + \Delta y^2} \tag{12}$$

$$r_1^2 = r_2^2 = L^2 + \Delta y^2 = r_c^2 \longleftrightarrow \Delta y^2 = r_c^2 - L^2 \tag{13}$$

With now only 3 ($\Gamma$, $r_c$ and $\Delta y$) unknown parameters it is possible to solve the equations.

Dividing Eq. 12 by Eq. 11 eliminates $\Gamma$. Inserting Eq. 13 gives:

$$\frac{V_{t,\Delta y}}{V_{t,\max}} = \frac{r_c \sqrt{r_c^2 - L^2}}{r_c^2 - \frac{L^2}{2}} \tag{14}$$

Equation 14 describes a tangential velocity ratio that is proportional to $L$. Also $L$ is known to range from 0 to $r_c$. A dimensionless relationship $L\, r_c^{-1}$ can be plotted and is shown in Fig. 11. By passing the vortex with $\Delta y < r_c$, and plotting the measured $V_t$ against the distance to the vortex (Fig. 10), we can determine $L, V_{t,\max}, V_t, \Delta y$. Using diagram Fig.11, we finally determine $L\, r_c^{-1}$ and thus $r_c$.

### 3.3 Analytical reconstruction

As shown above the presence and identification of a vortex (or a pair of vortices) is measurable. Basic geometry and the Burnham-Hallock model further allow for a reconstruction (analytical solution) of the individually measured vortex, which is helpful to verify the measurements and evaluation technique. With Eq. 15 and 16 the distance to each vortex core (centre) to and along the UAV flight path can be calculated (Fischenberg, 2011). In Fig. 12 the distances of the UAS to two vortices spinning in opposite direction are shown. In the figure vortex 1 is passed through its core and vortex 2 is passed with a slight off-set. The flight path of the UAS is indicated with a red dashed line. Those distances are inserted into Eq. 17 and 18 using

Wind Energ. Sci. Discuss., https://doi.org/10.5194/wes-2019-9
Manuscript under review for journal Wind Energ. Sci.
Discussion started: 1 March 2019
© Author(s) 2019. CC BY 4.0 License.

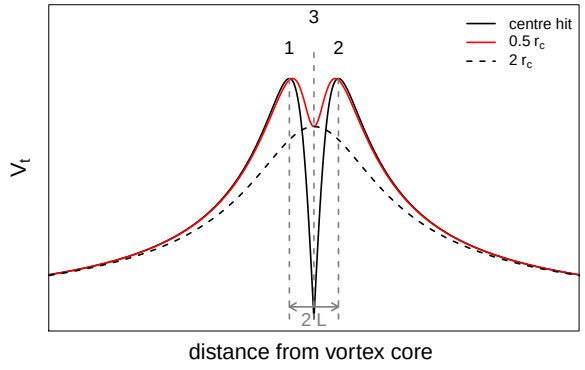


**Figure 10.** Analytical solution of a UAS passing the vortex at a path crossing the centre (black solid line), passing at $r = 0.5r_c$ (red line) and at a distance double the core radius (black dashed line). The peak to peak distance is 2 $L$ (cf. Fig. 9), above illustrated for the black solid line.

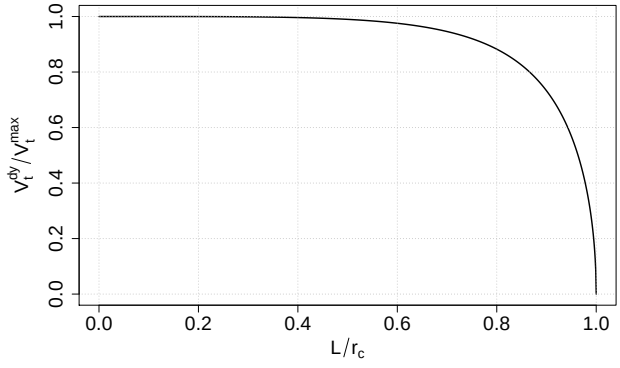


**Figure 11.** Dimensionless relationship between the ratio of the minimum (dent) tangential velocity and the maximum tangential velocity versus half the peak to peak distance ($L$) in percentage of $r_c$.

the relation of Eq. 4 the tangential velocity along the meteorological $x$ axis ($u$' component) and $y$ axis ($v$' component) can be calculated:

$$d_1 = \sqrt{\Delta x^2 + \Delta y^2} = \sqrt{(x - x_{\text{Vortex1}})^2 + (y - y_{\text{Vortex1}})^2} \tag{15}$$

$$d_2 = \sqrt{\Delta x^2 + \Delta y^2} = \sqrt{(x - x_{\text{Vortex2}})^2 + (y - y_{\text{Vortex2}})^2} \tag{16}$$

Wind Energ. Sci. Discuss., https://doi.org/10.5194/wes-2019-9
Manuscript under review for journal Wind Energ. Sci.
Discussion started: 1 March 2019
© Author(s) 2019. CC BY 4.0 License.

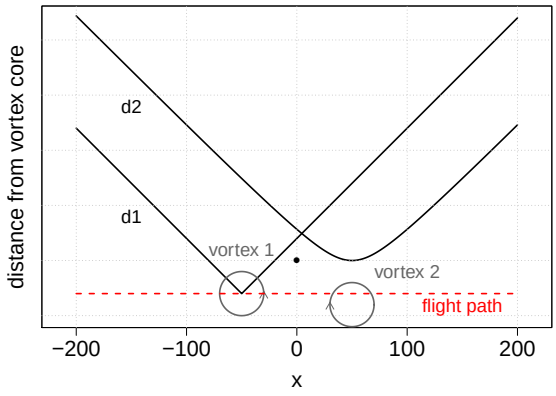


**Figure 12.** Qualitative example of an ideal flight path (vortex 1) and a passing with a little off-set (vortex 2) of the UAS. In a field measurement the distances $d1$ and $d2$ are calculated from the UAS GPS position and the location (off-set) of the vortex in relative coordinates with WEC at $(0,0)$, indicated with a black dot. The vortex position can be derived from the extent of the tangential velocity $V_\mathrm{t}$ measured by the UAS and the peak to peak distance explained in the previous sections. In this example $d_{1,2} = \sqrt{\Delta x^2 + \Delta y^2}$ with $\Delta y_1 = 0$ for $d1$ and $\Delta y_2 = \text{const.} \neq 0$ for $d2$.

While the $y$ coordinate can be derived from the measurement (using $\Delta y$ and the UAS position, s.a. chapter 4.2) the $x$ coordinate of the vortex $x_{\mathrm{Vortex1,2}}$ is the $x$ coordinate of the flight path at the position '3', e.g. Fig. 9.

$$u' = V_\mathrm{t}(d_1)\left(\frac{y - y_{\mathrm{Vortex1}}}{d_1}\right) - V_\mathrm{t}(d_2)\left(\frac{y - y_{\mathrm{Vortex2}}}{d_2}\right) \tag{17}$$

$$v' = -V_\mathrm{t}(d_1)\left(\frac{x - x_{\mathrm{Vortex1}}}{d_1}\right) + V_\mathrm{t}(d_2)\left(\frac{x - x_{\mathrm{Vortex2}}}{d_2}\right) \tag{18}$$

## 4 Results

### 4.1 Vortex measurement

Figure 13a shows the $v_\mathrm{h} = \sqrt{u^2 + v^2}$ component of the wind measurement behind the WEC at hub height. The data reveals several (near) wake specific features. This measurement shows two measurements of a tip vortex, indicated by the arrows in Fig. 13a. In-between those two peaks the wake deficit is measurable by a significant drop of the horizontal wind velocity. Due to the near vicinity to the nacelle the wake deficit is dominated by turbulence created by the blade root vortices.

Figure 14 shows a zoomed-in look at the measured vortices depicted in Fig. 13. Figure 14a shows the vortex measured while entering the wake (vortex 1) and 14b while leaving the wake (vortex 2). Both, (a) and (b), are the plain UAS measurements. Fig-

Wind Energ. Sci. Discuss., https://doi.org/10.5194/wes-2019-9
Manuscript under review for journal Wind Energ. Sci.
Discussion started: 1 March 2019
© Author(s) 2019. CC BY 4.0 License.

eawe european academy of wind energy
Open Access WIND ENERGY SCIENCE DISCUSSIONS

ure 14c and Fig. 14d show the same measurement but the UAS coordinate system is rotated into the vortex coordinate system. This ensures that the rotational energy of the vortex is entirely captured by the $u$ and $v$ component, thus becoming the velocity components of the two dimensional rotational plane of the vortex. Examining both vortices the velocity distribution pattern of the UAS passing at distance $r < r_\mathrm{c}$ is visible in the $v_\mathrm{h}$ measurement. The horizontal wind velocity $v_\mathrm{h}$ is a superposition of the tangential velocity, turbulence and the horizontal wind of the undisturbed inflow. The characteristics of the tangential velocity of vortex 1 (Fig. 14a,c) is almost solely determined by the *v* component, while in Fig. 14b,d the *u* component inheres an equal part. In the plain UAS measurement (i.e. before coordinate transformation) vortex 2 has a significant non-zero $w$ component (Fig. 14b), indicating that the vortex did not rotate in the $x-y$ plane, hence the coordinate transformation into the vortex coordinate system. Especially Fig. 14d shows a significant reduction of the $w$ component after the coordinate transformation. Purple dashed lines indicate the velocity deficit $dV_\mathrm{t}$ (dent), grey dashed lines the peak-to-peak distance. In Fig. 14 shown as a solid purple line. The dot-dashed purple line can be interpreted as an extension of the horizontal wind velocity by the $w$ component, essentially giving the norm of the wind vector:

$$|\boldsymbol{v}| = \sqrt{u^2 + v^2 + w^2} \tag{19}$$

The described coordinate system rotation was applied with respect to the area between the grey dashed lines (Fig. 14) i.e. between entering and leaving the vortex. A good indicator that the data rotation was successful is when the norm of the wind vector (purple dashed line) and the $v_\mathrm{h}$ in-between the grey dashed lines are about the same magnitude. Then it can be concluded that the two dimensional vortex rotation ($u$ and $v$ components) includes the entire kinetic energy, i.e. the vertical wind component is now neglectable.

Table 2 shows the derived parameters from the vortices depicted in Fig. 14. It has to be mentioned that vortex 1 made for a better and clearer measurement, since vortex 2 is influenced by the wind deficit and turbulence inside the wake. Vortex 1 shows a clear and sharp jump in the tangential velocity which makes it easier to obtain the necessary quantities and provides clearer results. Figure 16a shows the relationship between the velocity ratio (Eq. 14) at point 3 (cf. Fig. 10) and the peak to peak distance ($2\ L$) for the flight measurement. The obtained solutions for vortex 1 and 2 are marked with grey dashed lines. Equation 5 allows a calculation of $\Gamma$ from the parameters extracted from Tab. 2. The average of the obtained circulations is $\overline{\Gamma} = 74.17\ \mathrm{m^2\ s^{-1}}$, the average core radius is $\overline{r}_\mathrm{c} = 0.61\ \mathrm{m}$.

Figure 15 shows two dimensional cut through a skewed or canted vortex that results in an ellipse where the peak to peak distance is $2\ L'$. This peak to peak distance is under-predicted ($2\ L' < 2\ L$). The introduced error $\Delta y'$ is visualised in Fig. 15 by dotted red lines. To overcome this issue the measured data are rotated into the vortex hose if necessary. This simulates the UAS canting to follow the skewed vortex hose.

### 4.2 Vortex reconstruction

With all necessary quantities obtained from the measurement an analytical reconstruction of the vortices can be done. Figure 16b shows the distribution of the tangential velocity of a typical vortex at 0.25 D from the WEC derived from the measurement of vortex 1 (Fig. 14a). With $\overline{\Gamma}$ and $\overline{r}_\mathrm{c}$ retrieved from Tab. 2 the minimum measured tangential velocity between the two peaks

Wind Energ. Sci. Discuss., https://doi.org/10.5194/wes-2019-9
Manuscript under review for journal Wind Energ. Sci.
Discussion started: 1 March 2019
© Author(s) 2019. CC BY 4.0 License.

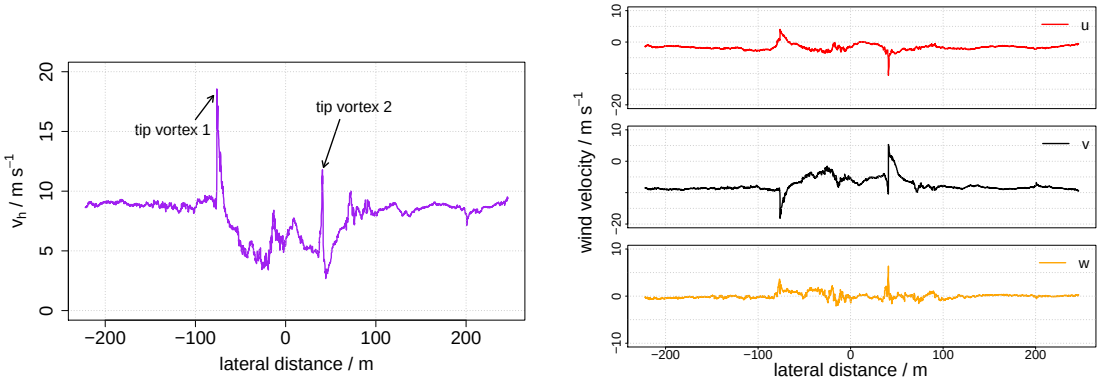


(a) (b)

**Figure 13.** (a) Horizontal wind $v_h$ measurement at hub height in the WEC wake at a distance of 0.25 D to the nacelle. The two tip vortices are indicated by the arrows. (b) The same measurement split into the three wind components $u, v, w$.

**Table 2.** Determined parameters from vortex measurements.

| Vortex | $dV_t$ [m s$^{-1}$] | $V_{t,max}$ [m s$^{-1}$] | $V_{t,\Delta y}$ [m s$^{-1}$] | $V_{t,\Delta y}/V_{t,max}$ [−] | $L$ [m] | $L/r_c$[−] | $r_c$ [m] | $\Gamma$ [m$^2$ s$^{-1}$] |
|---|---|---|---|---|---|---|---|---|
| Vortex 1 | 3.4 | 9.6 | 6.2 | 0.65 | 0.61 | 0.93 | 0.66 | 81.30 |
| Vortex 2 | 0.2 | 9.7 | 9.5 | 0.98 | 0.3 | 0.55 | 0.55 | 67.04 |

(position '3' in Fig. 14), a distance $\Delta y$ can be derived by comparing the measured tangential velocity with the analytical solution shown in Fig. 16b. The resulting distance to the vortex core $\Delta y$ can then be fed to a model, based on the Burnham-Hallock approach. Figure 17 shows the analytical solution of $u'$ and $v'$ overlain measured data of $u$ an $v$. Overlain to the in-situ data the tangential velocity still contains the mean horizontal wind $V_t = \sqrt{u'^2 + v'^2}$. For the analytical solution the measured data has been rotated slightly into the mean wind direction to fit the meteorological coordinate system with the vortex coordinate system, so the $u$ component equals zero in average and $v$ is the predominant horizontal wind direction. In addition to the solely Burnham-Hallock solution for the $v'$ component (dotted line in Fig. 17b) the long dashed line shows the same solution but multiplied with a correction factor to satisfy for the wind deficit in the wake. The general vortex model does not consider the mean horizontal velocity, so it needs to be accounted for, especially when there is a artificially induced drop behind the WEC in the wake. In the present case the velocity deficit was measured to be about 65 %. It is visible as a jump in the mean horizontal wind between the two measured vortices. This deficit is in agreement with the findings by Wildmann et al. (2014a) or Bartl et al. (2012). The velocity correction function is shown in Fig. 18 and is simply an upside down Tukey window. The analytical solution remains uncorrected until entering the wake of the WEC. After incorporating a deficit correction to the analytical solution it is visible that the deficit in the wake plays an important role to the structure of the vortex.

Wind Energ. Sci. Discuss., https://doi.org/10.5194/wes-2019-9
Manuscript under review for journal Wind Energ. Sci.
Discussion started: 1 March 2019
© Author(s) 2019. CC BY 4.0 License.

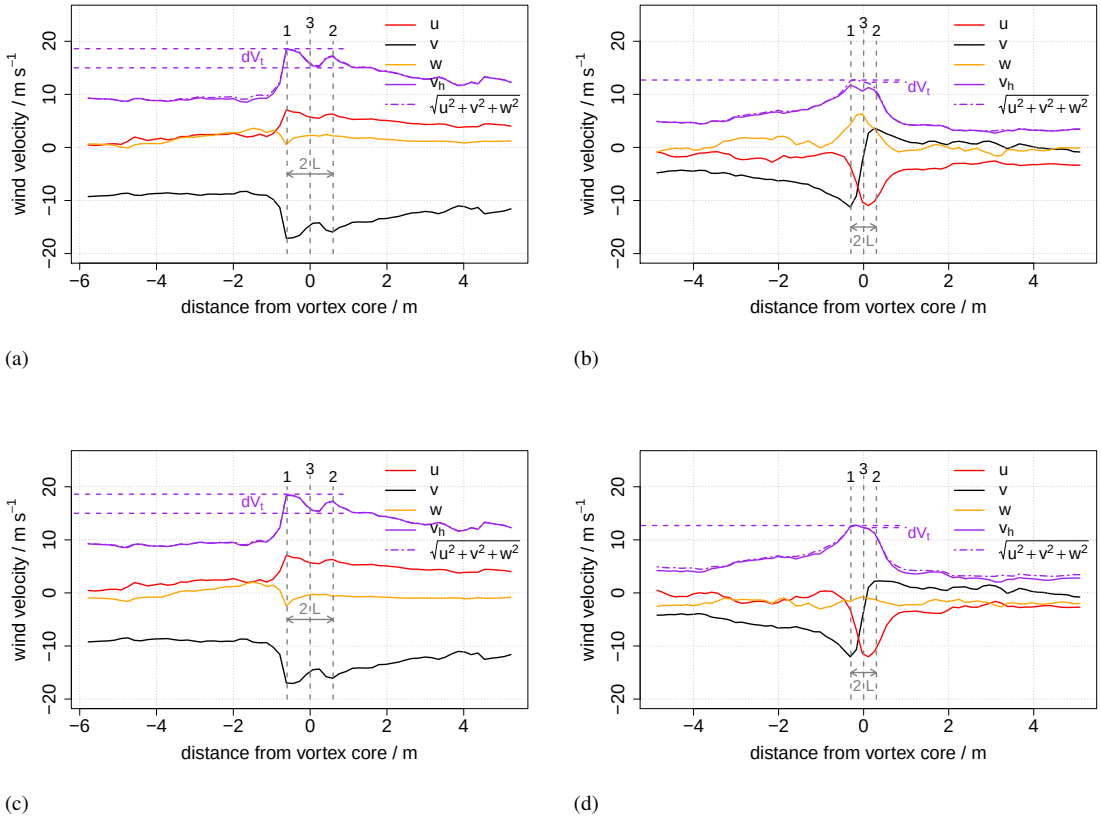


**Figure 14.** Measured tip vortex 1 and tip vortex 2 from Fig. 13a. Purple dashed lines indicate the velocity deficit (dent), grey dashed lines the peak-to-peak distance. The horizontal wind velocity $v_\mathrm{h}$ is a superposition of the tangential velocity and the horizontal wind of the inflow/surroundings. To eliminate the $w$ component the data has been rotated into the vortex coordinate system. This is necessary to measure the vortex correctly. The sub-figures (a) and (b) show the plain UAS measurement of the vortices. In sub-figures (c) and (d) the UAS has been rotated into the vortex coordinate system (vortex plane) to capture the whole two dimensional rotation.

Wind Energ. Sci. Discuss., https://doi.org/10.5194/wes-2019-9
Manuscript under review for journal Wind Energ. Sci.
Discussion started: 1 March 2019
© Author(s) 2019. CC BY 4.0 License.

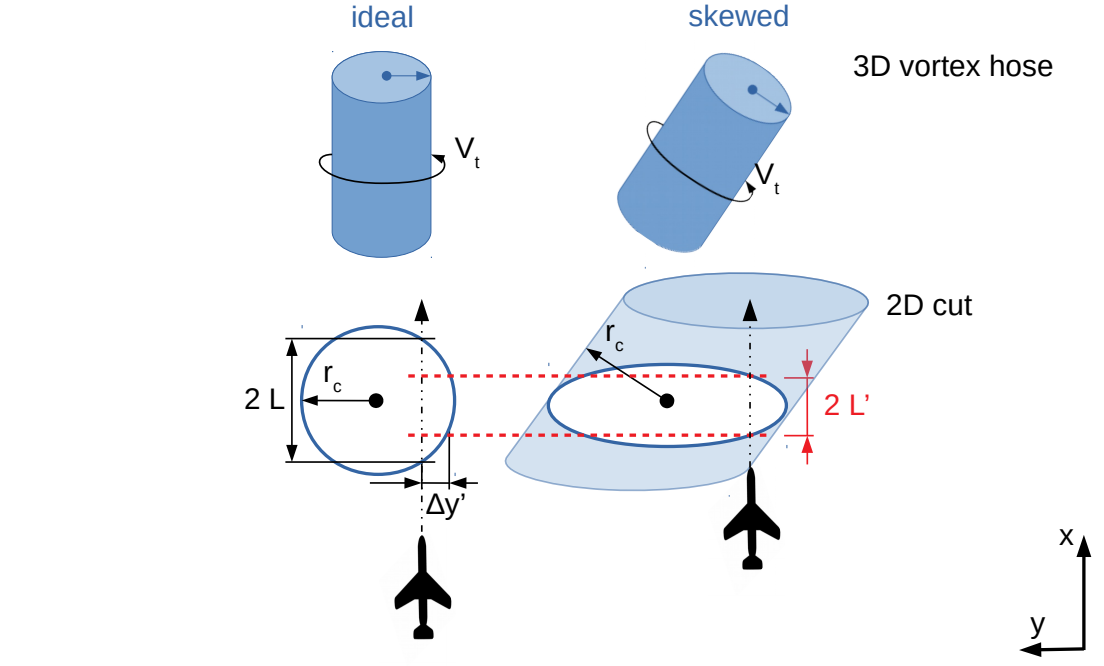


**Figure 15.** Sketch of an ideal and skewed (exaggerated) vortex hose at hub height. The simplifications in the evaluation method only consider components in the $x-y$ plane which leads to an under-prediction of the real peak to peak distance. The fact that the real '$r_c$' does not lie in the $x-y$ plane leads to an error. A horizontal cut though the vortex has an ellipsoidal geometry instead of a circular one as in ideal measurement conditions.

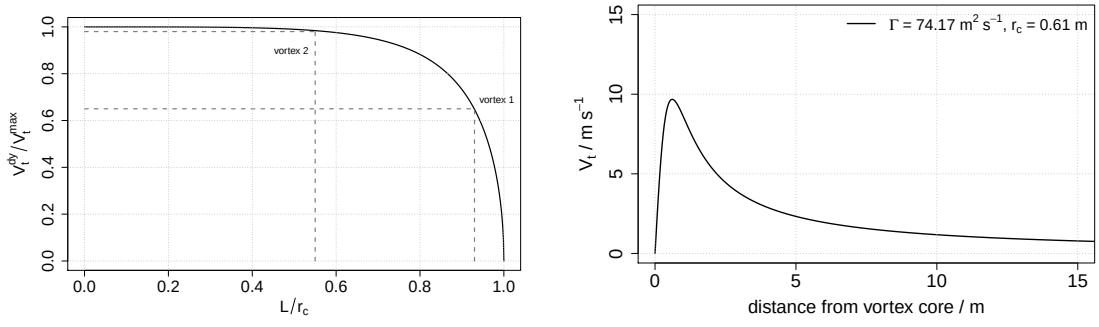


(a) (b)

**Figure 16.** (a) Obtaining the correction factor for $L$ for vortex 1 and 2 using the relationship described above. (b) Analytical solution for the tangential velocity of a vortex in the wake at a distance of 0.25 D. $\Gamma$ and $r_c$ averages from measurements from Tab. 2.

Wind Energ. Sci. Discuss., https://doi.org/10.5194/wes-2019-9
Manuscript under review for journal Wind Energ. Sci.
Discussion started: 1 March 2019
© Author(s) 2019. CC BY 4.0 License.

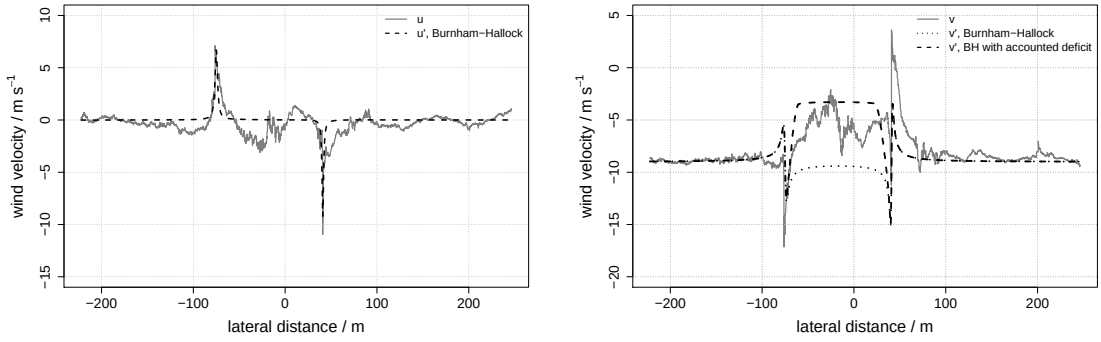


(a) (b)

**Figure 17.** Analytical solution (dashed lines) for $u'$ and $v'$ of the two vortices from the parameter evaluation (Fig. 14). The long dashed solution in (b) additionally accounts for the deficit in the wake.

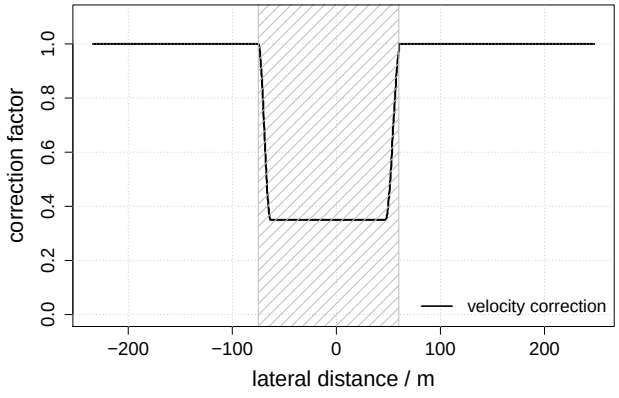


**Figure 18.** Velocity correction function for the $v'$ component of the analytical solution when entering the wake (grey).

## 5 Discussion

Here we compare the airborne measured circulation $\Gamma$ with data of the WEC itself and with data from an LES simulation. Equation 20 allows for a calculation of the blade tip vortex strength by given parameters (Sørensen et al., 2014):

$$\Gamma = \frac{\pi v_\infty^2 C_T}{\Omega N_\mathrm{b}} \approx 66.2\ \mathrm{m}^2\ \mathrm{s} \tag{20}$$

The rotational speed $\Omega$ is provided by the owner of the WEC. For the determination of the thrust coefficient $C_T$ the following estimation is done:

Wind Energ. Sci. Discuss., https://doi.org/10.5194/wes-2019-9
Manuscript under review for journal Wind Energ. Sci.
Discussion started: 1 March 2019
© Author(s) 2019. CC BY 4.0 License.

eawe european academy of wind energy
Open Access WIND ENERGY SCIENCE DISCUSSIONS

The relatively low wind speed ($v_\infty = 8.8\ \mathrm{m\ s^{-1}}$ by UAS measurement) implies a pitch angle of $\beta = 0°$ when approximating the E-112 with the NREL 5 MW offshore WEC (Jonkman et al., 2009).

The tip-speed ratio ($TSR = \frac{\Omega R}{v_\infty}$) can also be calculated and thus a thrust coefficient $C_T \approx 0.8$ can be estimated from the $C_T$ to $TSR$ relationship by Al-Solihat and Nahon (2018). With further $N_\mathrm{b}$ being the number of blades, $\Gamma$ can be calculated.

The calculated value for $\Gamma$ from WEC specific and atmospheric parameters is similar to the vortex strength that was extracted from the vortex measurement ($\overline{\Gamma} = 73.17\ \mathrm{m^2\ s^{-1}}$). This shows that the method presented here (calculation of Gamma from UAS data) provides reasonable results, and that the geometric simplification of the tip vortex and the application of the Burnham-Hallock model both are valid.

The Burnham-Hallock vortex model does work for aircraft induced vortices as shown by Ahmad et al. (2014) as well as Fischenberg (2011) and as the results imply, it can be used to describe WEC wake vortices. Not least, both phenomena can be described by two vortices spinning in opposite direction. Vortex patterns of a WEC wake show higher complexity than aircraft wake vortices. The whole wake is in motion and different turbulence and shear forces interact with each other. Therefore for the wake vortices some simplifications have to be made, e.g. the shown evaluation method is only valid for a 2-D cut of the whole vortex hose. Also the blade root vortex was not analysed any further.

In this study also the fact that the UAS experiences a change in true air speed (TAS) when entering the wake is ignored. Theoretically the calibration range of the used five hole probe is for a fixed air speed which changes when entering the wake. Since this evaluation uses the ratio of two velocities the influence of a different calibration for the five hole probe should not lead to a significant error. For the calculation of the circulation $\Gamma$, however, absolute velocities are necessary and a small error can be expected due to a change in TAS when entering the wake.

## 6 Conclusions and outlook

The resulting circulation strength $\Gamma$ derived from the data shows good accordance to the equation by Sørensen et al. (2014). This shows that the evaluation method using the basic geometrical properties of a vortex can be used to derive vortex properties in a flow. Turbulence acting on the vortex often aggravates an evaluation. So this method still has to be proven at larger distances to the WEC nacelle, where the vortices begin to meander and get unstable. However, to our knowledge, this is the first quantitative analysis of WEC tip vortices using in situ measured turbulence data.

The MASC Mk 3 system is capable of measuring detached tip vortices in the wake of a WEC. The spatial and temporal resolution is sufficient to detect vortex patterns in the measurements. However, on many occurrences the measured side slip angle beta overstepped the calibration of the 5-hole probe and in conclusion those measurements could not been used. This adds uncertainties to the wind measurement. For the measurements shown in this study the angles of the 5-hole probe were not exceeded. For future measurements the calibration of the 5-hole probes could simply be expanded to larger angles. This also allows for a lower TAS (true air speed) of the UAV, which in turn results in a better spacial resolution of the data. The path accuracy of the UAS will be upped by using an RTK GPS as originally intended.

Wind Energ. Sci. Discuss., https://doi.org/10.5194/wes-2019-9
Manuscript under review for journal Wind Energ. Sci.
Discussion started: 1 March 2019
© Author(s) 2019. CC BY 4.0 License.

eawe european academy of wind energy
Open Access WIND ENERGY SCIENCE DISCUSSIONS

The proposed analytical vortex model by Burnham and Hallock is capable of describing WEC wake vortices. Yet, as for most analytical models, the analytical solution shown in this paper can and should be improved. E.g. to better fit the WEC wake (velocity deficit, blade root vortex near the nacelle). This evaluation was conducted with data obtained at 0.25 D from the nacelle. For a future additional field campaign blade tip vortices in the farther wake shall be investigated.

*Competing interests.* The author declares that he has no competing interests.

*Acknowledgements.* We acknowledge support by Projekträger Jülich and the BMWi (Federal Ministry for Economic Affairs and Energy) that funded the HeliOW project. We thank Enercon GmbH for cooperation and WRD GmbH for the provision of a generic recreation of the E-112 geometry for the numerical simulations. We also acknowledge support by Deutsche Forschungsgemeinschaft and Open Access Publishing Fund of University of Tübingen. For extensive technical support at the field campaign I want to thank Martin Schön and Patrick Manz.

Wind Energ. Sci. Discuss., https://doi.org/10.5194/wes-2019-9
Manuscript under review for journal Wind Energ. Sci.
Discussion started: 1 March 2019
© Author(s) 2019. CC BY 4.0 License.

eawe european academy of wind energy
Open Access WIND ENERGY SCIENCE DISCUSSIONS

## References

Ahmad, N. N., Proctor, F. H., Duparcmeur, F. M. L., and Jacob, D.: Review of Idealized Aircraft Wake Vortex Models, 52nd AIAA Aerospace Sciences Meeting; 13-17 Jan. 2014; National Harbor, MD; United States, 2014.

Al-Solihat, M. K. and Nahon, M.: Flexible Multibody Dynamic Modeling of a Floating Wind Turbine, International Journal of Mechanical Sciences, 142–143, 518–529, https://doi.org/10.1016/j.ijmecsci.2018.05.018, 2018.

Bartl, J., Pierella, F., and Sætrana, L.: Wake Measurements Behind an Array of Two Model Wind Turbines, Energy Procedia, 24, 305 – 312, https://doi.org/https://doi.org/10.1016/j.egypro.2012.06.113, http://www.sciencedirect.com/science/article/pii/S1876610212011538, selected papers from Deep Sea Offshore Wind R&D Conference, Trondheim, Norway, 19-20 January 2012, 2012.

Burnham, D. C. and Hallock, J. N.: Chicago Monoacoustic Vortex Sensing System, Wake Vortex Decay, 4, 590–599, 1982.

Cormier, M., Caboni, M., Lutz, T., Boorsma, K., and Krämer, E.: Numerical analysis of unsteady aerodynamics of floating offshore wind turbines, Journal of Physics: Conference Series, 1037, 072 048, http://stacks.iop.org/1742-6596/1037/i=7/a=072048, 2018.

Fischenberg, D.: Charakterisierung von Wirbelschleppen aus In-Situ-Flugmessdaten der Falcon D-CMET, Tech. rep., DLR Institut für Flugsystemtechnik, https://elib.dlr.de/70300/, 2011.

Jeong, J. and Hussain, F.: On the identification of a vortex, Journal of fluid mechanics, 285, 69–94, 1995.

Jonkman, J., Butterfield, S., Musial, W., and Scott, G.: Definition of a 5-MW Reference Wind Turbine for Offsore System Development, Technical report, National Renewable Energy Laboratory, 2009.

Kim, Y., Jost, E., Bangga, G., Weihing, P., and Lutz, T.: Effects of ambient turbulence on the near wake of a wind turbine, Journal of Physics: Conference Series, 753, 032 047, http://stacks.iop.org/1742-6596/753/i=3/a=032047, 2016.

Kroll, N. and Fassbender, J. K.: MEGAFLOW - Numerical Flow Simulations for Aircraft Design, Springer Verlag GmbH, 2005.

Lamb, H.: Hydrodynamics, Cambridge University Press, 1939.

Menter, F.: Two-equation eddy-viscosity turbulence models for engineering applications, AIAA Journal, 32, https://doi.org/https://doi.org/10.2514/3.12149, 1994.

Sørensen, J. N., Mikkelsen, R., Sarmast, S., Ivanell, S., and Henningson, D.: Determination of Wind Turbine Near-Wake Length Based on Stability Analysis, Journal of Physics: Conference Series, 524, 012 155, http://stacks.iop.org/1742-6596/524/i=1/a=012155, 2014.

Subramanian, B., Chokani, N., and S. Abhari, R.: Drone-Based Experimental Investigation of Three-Dimensional Flow Structure of a Multi-Megawatt Wind Turbine in Complex Terrain, Journal of Solar Energy Engineering, 137, 2015.

Vermeer, N.-J.: Local circulation on rotating wind turbine blades from velocity measurements in the wake of a model rotor, British Wind Energy Association AnnualWind Energy Conference 1992, pp. 117–121, 1992.

Wildmann, N., Hofsäß, M., Weimer, F., Joos, A., and Bange, J.: MASC; a small Remotely Piloted Aircraft (RPA) for wind energy research, Advances in Science and Research, 11, 55–61, https://doi.org/10.5194/asr-11-55-2014, http://www.adv-sci-res.net/11/55/2014/, 2014a.

Wildmann, N., Ravi, S., and Bange, J.: Towards higher accuracy and better frequency response with standard multi-hole probes in turbulence measurement with remotely piloted aircraft (RPA), Atmospheric Measurement Techniques, 7, 1027–1041, https://doi.org/10.5194/amt-7-1027-2014, http://www.atmos-meas-tech.net/7/1027/2014/, 2014b.

Zhang, W., Markfort, C. D., and Porté-Agel, F.: Near-wake flow structure downwind of a wind turbine in a turbulent boundary layer, Experiments in Fluids, 52, 1219–1235, https://doi.org/10.1007/s00348-011-1250-8, 2012.